ASTRONOMY & ASTROPHYSICS
SUPPLEMENT SERIES

Astron. Astrophys. Suppl. Ser. **135**, 511–529 (1999)

The Hamburg/SAO Survey for Emission–Line Galaxies

I. A First List of 70 Galaxies

A.V. Ugryumov[1], D. Engels[2], V.A. Lipovetsky[1,⋆], H.-J. Hagen[2], U. Hopp[3,8], S.A. Pustilnik[1], A.Yu. Kniazev[1], G. Richter[4], Yu.I. Izotov[5], and C.C. Popescu[6,7]

[1] Special Astrophysical Observatory, Nizhnij Arkhyz, Karachai-Circessia 357147, Russia
[2] Hamburger Sternwarte, Gojenbergswerg 112, D-21029 Hamburg, Germany
[3] Universitäts-Sternwarte, Scheiner Str. 1, D-81679 München, Germany
[4] Astrophysikalisches Institut Potsdam, An der Sternwarte 16, D-14482 Potsdam, Germany
[5] Main Astronomical Observatory, Goloseevo, Kiev-22 252650, Ukraine
[6] Max-Planck Institut für Kernphysik, Saupfercheckweg 1, D-69117 Heidelberg, Germany
[7] The Astronomical Institute of the Romanian Academy, Str. Cuţitul de Argint 5, 75212 Bucharest, Romania
[8] Visiting astronomer at Calar Alto Observatory, Spain

Received August 28; accepted November 23, 1998

Abstract. We present first results[1] of the Hamburg/SAO Survey for Emission-Line Galaxies (HSS therein, SAO – Special Astrophysical Observatory, Russia) which is based on the digitized objective-prism photoplates database of the Hamburg Quasar Survey (HQS). The main goal of this survey is the search for emission-line galaxies (ELG) in order to create a new deep sample of blue compact galaxies (BCG) in a large sky area. Another important goal of this work is to search for new extremely low-metallicity galaxies. We present the first results of spectroscopy obtained with the 2.2 m telescope at the German-Spanish Observatory at Calar Alto, and with the 6 m telescope at the Russian Special Astrophysical Observatory. The primary ELG candidate selection criteria applied were a blue continuum (near λ 4000 Å) and the presence of emission lines close to λ 5000 Å recognized on digitized prism spectra of galaxies with magnitudes in the range $B = 16\overset{\mathrm{m}}{.}0 - 19\overset{\mathrm{m}}{.}5$. The spectroscopy resulted in the detection or/and quantitative spectral classification of 74 emission-line objects. Of them 55 are newly discovered, and 19 were already known as galaxies before. 11 of the latter have redshifts and are known ELGs. For most of the known galaxies emission line ratios were measured for the first time and an improved classification is presented. 47 objects are classified as BCGs, one as Sy2 galaxy, six as possible LINERs, and four as new QSOs. The remaining galaxies do not show significant Hβ and [OIII] $\lambda\lambda$ 4959, 5007 Å emission lines, and are likely either low-ionization starburst or dwarf amorphous nuclear starburst galaxies.

Key words: surveys — galaxies: fundamental parameters — galaxies: distances and redshifts — galaxies: starburst — galaxies: compact

1. Introduction

Since the pioneering work of Markarian (1967) objective prism surveys were recognized as a powerful tool to search for galaxies of various types of activity. As the result of nearly a dozen large objective prism surveys completed during the two last decades the main statistical properties were derived for various types of AGNs and for galaxies with enhanced current star formation.

While the selection of objects from objective prism spectra by their enhanced UV continuum was the primary criterion applied by Markarian (1967) and has proven to be especially efficient in searching for new Seyfert galaxies and QSOs, as well as for various types of star forming (SF) galaxies, the selection on the base of strong emission lines was shown to be also very efficient both in search for AGNs and galaxies with strong current star formation.

Several large samples of such galaxies have appeared as the results of University of Michigan (UM), Tololo & Calan-Tololo (Smith et al. 1995; Salzer & MacAlpine 1988; Salzer 1989b; Terlevich et al. 1991; Maza et al. 1991), Case (Salzer et al. 1995), Second Byurakan (SBS) Izotov

Send offprint requests to: and@sao.ru

⋆ Deceased September 22, 1996.

[1] Tables 1 to 5 are only available in electronic form at the CDS via anonymous ftp to cdsarc.u-strasbg.fr (130.79.128.5) or via http://cdsweb.u-strasbg.fr/Abstract.html

et al. 1993a; Stepanian 1994; Pustilnik et al. 1995), and the Heidelberg void survey (Popescu et al. 1996, 1997, 1998).

Of special interest are blue compact galaxies (BCGs). They are underluminous galaxies with an intense star formation burst taking place currently. BCGs are in general blue ($B - V < 0.5$), have small sizes (typically less than 10 kpc), low metallicity ($Z < 1/3\ Z_\odot$) and are gas-rich (Thuan & Martin 1981). They attracted much attention since their first description by Sargent & Searle (1970). Even earlier, these galaxies were recognized as objects which deserve attention in works by Haro (1956), Zwicky (1964) and Markarian (1967). As most of the BCGs have strong emission lines they can be classified as HII-galaxies as well (Veilleux & Osterbrock 1987). In this and following papers we will use the term BCG for designation of blue compact galaxies with HII-type emission-line spectra.

There are several important aspects in studies of BCGs. Searle & Sargent (1972) have noted that they can be truly young galaxies, forming their first stars. The outstanding examples of such objects are I Zw 18 (Sargent & Searle 1970; Kunth et al. 1995) and SBS 0335−052 (Izotov et al. 1990; Izotov et al. 1997a) with metallicities of $1/50\ Z_\odot$ and $1/41\ Z_\odot$, respectively. Another intriguing question is on possible evolutionary links of BCGs with other types of low-mass galaxies (dEs, dIs, LSBDs (see, e.g. Davies & Phillips 1989)). The spatial distribution of low-mass galaxies is still debated in connection with predictions for various models of galaxy formation (Bardeen et al. 1986; Dekel & Silk 1986). Despite of 10 years studies (Salzer 1989b; Thuan et al. 1991; Weinberg et al. 1991; Rosenberg et al. 1994; Pustilnik et al. 1995; Popescu et al. 1997) there is still no self-consistent picture. The strong emission lines in the spectra of BCGs allow to detect them easily far beyond the Local Supercluster. This advantage is very important for compiling large (covering over ∼1000 square degrees) and relatively deep ($z \sim 0.03 - 0.04$) samples to study statistical properties of low-mass galaxies, their space distribution and luminosity function, their star formation rate and to find more extremely low-metallicity galaxies.

There are at present several large BCG samples on the Northern sky at high latitude. One of them includes ∼240 objects in the region of the SBS survey (Markarian et al. 1983, 1987) $\alpha = 7^{\rm h}40^{\rm m} - 17^{\rm h}20^{\rm m}$, $\delta = 49^\circ - 61.2^\circ$ within an area of about 1000 square degrees (Izotov et al. 1993a,b; Pustilnik et al. 1995) and is based on ELGs selected by the SBS and the First Byurakan survey (FBS; Markarian catalog; Markarian et al. 1989; Mazzarella & Balzano 1986) (hereafter this sample is referred to as the SBS sample). Another sample is based on the galaxies found in the Case Northern sky objective prism survey (see Pesch et al. 1995 for the most recent reference). This BCG sample in the sky region of $\alpha = 8^{\rm h} - 16^{\rm h}$, $\delta = +29^\circ - +38^\circ$ was recently presented by Ugryumov (1997). The sample was created on results of follow-up spectroscopy with the 6 m Russian telescope by Ugryumov et al. (1998) and incorporates the results of earlier spectroscopy of Case ELG candidates by Augarde et al. (1987), Weistrop & Downes (1988, 1991) and Salzer et al. (1995) (hereafter this sample is referred to as the Case sample). A third sample of BCGs of Popescu et al. (1997, 1998) contains about 200 BCGs distributed in four regions of the northern sky and is based on a sample selected on the Hamburg Quasar Survey (HQS; Hagen et al. 1995) digitised IIIa-J plates.

Between the above mentioned surveys still exists a large area in the sky not yet totally covered (see Fig. 6). A minor part of this region was covered by the survey of Popescu et al. (1997, 1998). It was tempting to cover this gap with a new ELG survey using also the HQS objective prism plates, thus extending the survey of Popescu et al. (1997, 1998). The new project — the Hamburg/SAO survey for emission-line galaxies (HSS) — aims to create a new large and deep BCG sample in the area $7^{\rm h}20^{\rm m} < \alpha < 17^{\rm h}40^{\rm m}$, $35^\circ < \delta < 50^\circ$.

In this paper we describe the general outline of the project and present first results, which are used to improve the selection efficiency for the following parts of the survey. In Sect. 2 the selection criteria are discussed, in Sect. 3 the follow-up spectral observations and data reduction are described. We present the results and analysis of spectrophotometric observations in Sect. 4. The efficiency of the survey in BCG detection, and future perspectives are discussed in Sect. 5. In Sect. 6 we summarise the first results of the survey. Throughout this paper a Hubble constant of $H_0 = 75\ {\rm km\,s^{-1}\ Mpc^{-1}}$ is used.

2. Selection of ELG candidates from objective prism spectra

The ELG candidates were selected from the digitized objective prism plates of the Hamburg Quasar Survey. The original plates were obtained with the 80 cm Schmidt telescope at Calar Alto, Spain. The telescope is equipped with an 1.7° objective prism allowing to obtain spectra with a dispersion of ∼1390 Å/mm at Hγ. The size of plates is 24 × 24 cm covering a field of 5.5° × 5.5° on the sky. The Kodak IIIa-J emulsion is used, giving a spectral range from 3400 to 5400 Å. The plates were digitized with a PDS 1010 G microdensitometer in a low-resolution mode using 100 × 20 μm slit and 10 μm step size and the extracted spectra are stored on optical disks. Once spectra of candidates are taken from this database, high-resolution PDS scans (with a slit size of 20 × 20 μm) are made of them for further refinement of the classification. Additional information about the HQS can be obtained from Hagen et al. (1995). The low-resolution spectra, which have 10 − 20 spectral points per object, already allow the detection of strong emission lines, in particular

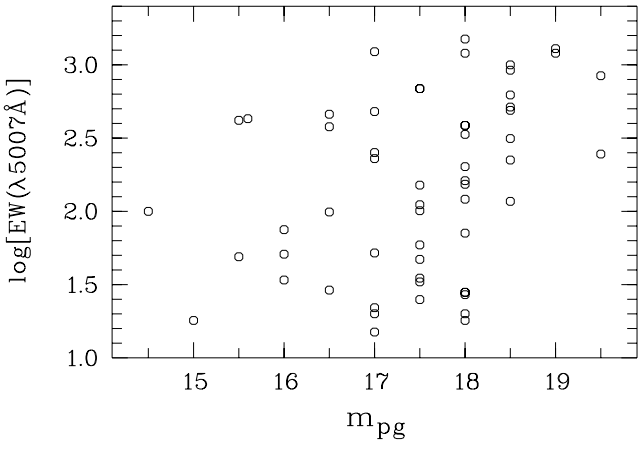

Fig. 1. Distribution of equivalent widths of the [OIII] λ 5007 Å emission line in Å as function of photographic magnitude for the training sample of known BCGs

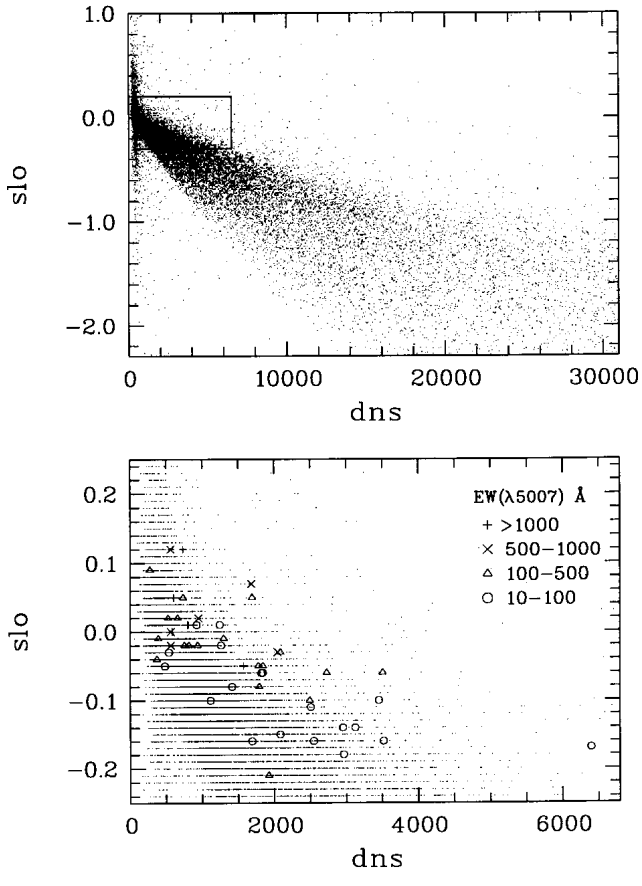

Fig. 2. Positions of known BCGs from the training sample in the unitless coordinates integral density (brightness) (dns) — slope of spectra (slo) (large symbols) compared to objects of all types as recorded from the HQS plates. The various symbols denote different ranges of the equivalent width of the [OIII] λ 5007 Å emission line. The lower part of the figure is a magnified part of the upper panel within the rectangle. This rectangle indicates our final selection box (see text for details)

for ELGs with prominent [OIII] $\lambda\lambda$ 4959, 5007 Å and Hβ lines. The faintest ELG candidates have B magnitudes up to $20^{\rm m}$. In general their redshifts are limited to $z \leq 0.075$ because the [OIII] $\lambda\lambda$ 4959, 5007 Å lines are shifted for more distant galaxies outside the spectral range of the photoplates. Sometimes prominent Hβ may allow detection up to $z \leq 0.1$, and in rare cases galaxies may be selected due to their strong [OII] λ 3727 Å emission line up to a redshift of $z = 0.43$. The selection is biased for the [OIII] lines compared to the [OII] line because of linear dispersion, favoring the detection of narrow lines near the red end of the objective prism spectra. Only in bright galaxies ($B < 17\overset{\rm m}{.}5$) the [OII] line was well detected (for example, HS 0132+0610 and HS 0935+4726, see Vogel et al. 1993). Quasars with strong emission lines near λ 5000 Å can also be detected, in particular, if Lyα λ 1216 Å or MgII λ 2798 Å enter to this wavelength region (corresponding to redshifts of $\sim$3.0 and 0.9, respectively).

The adopted search method consists of various selection techniques. It is applied first to the low-resolution and subsequently to the high-resolution density spectra. The low-resolution density spectra are characterized by several parameters, and we chose after some experiments the integral density and the slope at 4000 Å as the main selection parameters. The integral density is the sum of the densities of all pixels contributing to a spectrum and the slope is determined by a 2nd order polynomial fitting of the spectrum. The length of the selected spectra was limited to $5 - 20$ pixels to avoid spectra dominated by noise or affected by overlaps. To determine the range of slopes shown by ELGs for a given brightness (represented by the integral density), we used a training sample of $\sim$50 blue compact galaxies with known spectral properties taken from the SBS (Izotov et al. 1993a, 1994), which were separated on HQS plates in the zone of the SBS. This sample contains galaxies with a wide range of sizes, luminosities and [OIII] λ5007 Å emission line equivalent widths between 10 and more than 1000 Å. Figure 1 shows the distribution of the training sample in a photographic magnitude – equivalent width plane. For magnitudes fainter than about $18\overset{\rm m}{.}0$, our training sample is running out of objects with moderate or weak [OIII] line strength. This yielded some uncertainties at the fainter end for our first definition of the selection rules (see below).

Figure 2 shows the location of the SBS BCGs in an integral density – slope diagram (in the relative units of the digitisation of the HQS plates). According to the distribution of BCGs in this diagram we chose limits $-0.3 \div 0.15$ for the slope and $400 \div 6500$ for the densities. The slope range is rather wide due to both the intrinsic properties of the galaxies and variations of the plates quality. Nearly 30% of the typically $30000 - 50000$ spectra per plate pass this filter. This number of spectra is still too large to proceed with high-resolution scans. Therefore, all preselected low-resolution spectra were visually classified on a vector graphics screen and candidates with density peaks close

to the green head of the spectrum were selected as possible [OIII] λ5007 Å hits. This procedure is quite efficient to keep good ELG candidates and to reduce the total number of selected candidates to $3000 \div 5000$. Tests with several plates of the same field have shown that 5 to 15% of good candidates are lost, if the selection was not made on the best plate.

All selected low-resolution spectra were then rescanned with high resolution (PDS scanning time ∼3–4 hours/plate) in order to select visually first and second priority candidates according to the following criteria:

a) Objects showing a clear density peak near 5000 Å and blue continuum in the high resolution spectra are adopted as first priority candidates.

b) Some bright ($B \leq 18\overset{\mathrm{m}}{.}5$) BCGs with weaker emission lines (EW([OIII] λ5007 Å) $\sim$ 50 Å) in the training sample have density spectra with blue continuum but no clearly detectable emission peak. Therefore, candidates with a blue continuum but without prominent emission features or candidates with indications of emission peaks but with an unusual continuum shape are kept as second priority candidates in the attempt to avoid losses of true ELGs.

Examples of the high resolution spectra of the first and the second priority candidates are shown in Fig. 3 (small boxes include the low resolution spectra). As a result we have got up to 30 first priority candidates per plate and a similar number of second priority objects for follow-up spectroscopy. The resulting surface density of emission-line candidates for each priority varies from 0.3 to 1 candidate per square degree.

It is reasonable to outline here the ELG types which we wish to discriminate with the selection procedure used. First, due to the adopted slope limits of the spectra in the parameter space, we miss ELGs with redder continuum distribution. This is usually the case for galaxies dominated by the emission of an old stellar population. Such objects are found efficiently using wide-field objective prism surveys sensitive to the Hα spectral range (Zamorano et al. 1994, 1996) or by surveys based on narrow-band Hα imaging (Boroson et al. 1993). Second, due to the combined effect of the upper limit on the redshift of [OIII] $\lambda\lambda$ 4959, 5007 Å and the lower limit on the object's apparent magnitude (corresponding to the upper limit in integral density), we miss all objects with absolute magnitudes brighter than $M_B \sim -21$. Therefore, many Seyfert galaxies are not selected into our candidate lists.

We apply the above selection procedure to the first set of 38 fields with boundaries $\alpha = 8^{\mathrm{h}} - 17^{\mathrm{h}}30^{\mathrm{m}}, \delta = +45^{\circ} - +50^{\circ}$ and $\alpha = 8^{\mathrm{h}} - 15^{\mathrm{h}}30^{\mathrm{m}}, \delta = +40^{\circ} - +45^{\circ}$, comprising an area of about 900 square degrees. This survey strip partly overlaps with the fields of Popescu et al. (1996, 1997). The resulting list consists of about 1000 first priority candidates, and a similar number of second priority ones. To check the contents of these categories we observed both first and second priority candidates in two

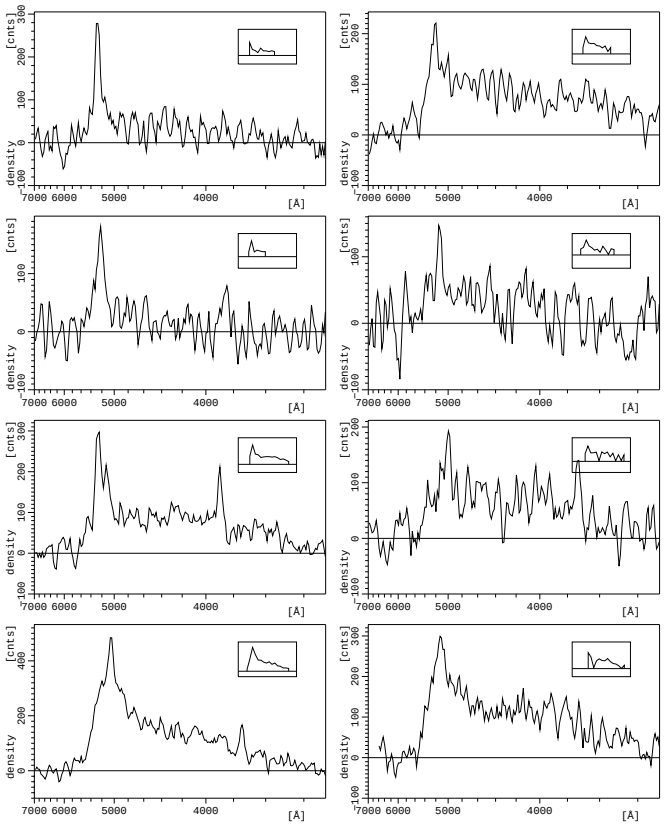

Fig. 3. Examples of candidates selected as first (left panel) and second (right panel) priorities. The high resolution scans are shown, the inlets present the low resolution scans used for the first selection step. For details see text

pilot follow-up spectroscopy runs. The candidate lists contain also many ELGs with known redshifts but with somewhat uncertain classification. Due to the lack of time we could observe only 11 of them.

After the analysis of the results of these observations (see Sect. 5), we improved the efficiency of the overall selection procedure by applying additional criteria, which resulted in a significant increase of ELG detection efficiency during follow-up spectroscopy.

3. Spectral observations and data reduction

3.1. SAO 6 m observations

The first observations of a small subsample of HSS candidates were conducted in January 1995 with the SAO 6 m telescope. The telescope was equipped with the 1024-channel photon counter detector (IPCS) mounted on the medium resolution spectrograph SP-124 in the Nasmyth-1 focus (Drabek et al. 1986). A 2″ diameter circular aperture was centered on the brightest part of the target galaxy or on the star-like candidate, and a similar aperture was

placed 20″ off along the direction zenith-nadir to accumulate simultaneously the night sky spectrum. The latter was subtracted during the data reduction from the target spectrum. This set-up resulted in a spectral coverage of λ 3700 – 5500 Å with a scale 1.8 Å/channel along the dispersion and a spectral resolution (FWHM) of about 10 Å. The exposure time varied between 3 and 5 min depending on the brightness. The signal-to-noise ratios of these spectra are ≈5 in the continuum at λ 5000 Å. The seeing was about 2″.

During the night we have observed spectrophotometric standards from the KPNO list (Massey et al. 1988) which were used to correct the spectra of the program galaxies for the system spectral response. An Ar-Ne-He lamp was used for the wavelength calibration. A flat-field was accumulated every night before and after the observations and all spectra are corrected for the flat field after azimuth and modulation correction of the original 1024-channel arrays.

3.2. Calar Alto 2.2 m observations

Further follow-up spectroscopy was made during nights May 30 – June 4, 1995, using the Boller & Chivens spectrograph attached to the Cassegrain focus of the Calar Alto 2.2 m telescope. A 300″ × 2″ long slit was used. The spectra were recorded on a 1024 × 1024 pixel Tektronix CCD operated in a 2 × 1 binned mode (binning only along the slit direction), resulting in a spectral resolution of 9 Å and a wavelength coverage λ 3700 – 8100 Å. The exposure times varied between 2.5 and 15 min depending on the galaxy brightness. The observations were complemented by standard star flux measurements, lamp exposures for wavelength calibration, dome flats, bias and dark frames. The seeing was mostly about 1″, rising at times up to 2″. The observations during the second and the last night were made under non-photometric conditions. The flux calibration for the dozen objects observed during the second half of the last night is especially uncertain.

3.3. Data reduction

Data reduction was done at SAO with the MIDAS 94NOV software package. The context SPEC is adapted to the SAO data formats to perform an automatic reduction of the one-dimensional IPCS spectra (Kniazev 1994). Corrections for flat field, azimuthal shift and two-channel modulation are applied to the IPCS spectra. Then, standard corrections for the atmospheric extinction, sky subtraction, and the instrumental response curve are done. All the IPCS spectra were taken mainly during rather poor, non-photometric weather conditions and, therefore, are presented in a relative count scale.

For the Calar Alto two-dimensional CCD data, the reduction included bias-dark correction, cosmic-ray removal and flat-field correction. 1-D spectra are extracted by adding 3 – 4 consecutive CCD rows centered at the object intensity peak. After sky subtraction they are converted to linear scale and corrections for atmospheric extinction and flux calibration are applied. For the flux calibration we use the mean response curve obtained from observations of two standard stars. Calar Alto CCD spectra are presented on an absolute flux scale.

The redshifts and line fluxes are measured applying Gaussian fits to the line profiles. The average redshift of each galaxy is derived from the observed wavelengths of all prominent individual emission lines excluding [OII] λ 3727 Å, which is outside of the region where the wavelength calibration curve is well determined. The typical internal redshift errors are estimated to be less than 0.0001 for the Calar Alto emission-line spectra and less than 0.0003 for the 6 m emission-line spectra. For galaxies with absorption features the redshift errors are within ∼0.0005.

The emission line fluxes are derived as the sum of the pixel intensities inside the line region using standard MIDAS program tools. For all but one spectrum, the individual emission line fluxes of the Hα, [NII] $\lambda\lambda$ 6548, 6583 Å and [SII] $\lambda\lambda$ 6716, 6731 Å line blends are obtained by summing of pixel intensities over the total blend and then modelling the individual line fluxes using Gaussian fitting.

4. Results of follow–up spectroscopy

In total 216 candidates were observed during the January – June, 1995, of which 33 objects were observed with the 6 m telescope, 183 objects with the Calar Alto 2.2 m telescope, and 4 with both instruments. Due to the schedule of the observations almost all candidates are located in the region $\alpha = 12^{\rm h} - 17^{\rm h}$ and $\delta = +45° - +50°$. We find 59 new emission line galaxies, 4 quasars and 7 galaxies with absorption lines. For 11 of the known ELGs we measure emission line ratios and make quantitative classification. The remaining objects are stars or they have featureless spectra with signal-to-noise ratios insufficient to detect weak lines. The overall detection efficiency of emission-line objects (calculated after exclusion of 11 known ELGs) is rather low for this first sample, (63/205 or 30.7%). This is especially true when compared with the efficiency from Popescu et al. (1997) of about 76%, for the same photographic plates. Nevertheless, we will improve on it by including additional selection criteria, as will be discussed in Sect. 5.3.

4.1. Emission-line galaxies

The new emission-line galaxies are listed in Table 1, containing the following information:
Column 1: The object's IAU-type name with the prefix HS.

Columns 2 and 3: Right ascension and declination for epoch B1950. The coordinates are measured on direct plates of the HQS and are accurate to $\sim 2''$ (Hagen et al. 1995).
Column 4: Heliocentric velocity. Typical accuracy is between 30 and 90 km s^{-1}.
Column 5: Apparent B magnitude, as obtained by the calibration of the digitized photoplates (Engels et al. 1994). It has an rms accuracy of $\sim 0\overset{m}{.}5$ for objects fainter than $m_B = 16\overset{m}{.}0$ (Popescu et al. 1996). Magnitudes marked by an asterisk are taken from the APM survey (Maddox et al. 1990). Since the calibration algorithm is optimized for point sources the brightness of extended galaxies is underestimated. We expect that uncertainties of the magnitudes can be up to 2 mag (Popescu et al. 1996).
Column 6: Absolute B magnitude calculated from the apparent B magnitude and the heliocentric velocities. No correction for galactic extinction is made because all observed objects are located at high galactic latitudes and because the corrections are significantly smaller than the uncertainties of the magnitudes.
Column 7: Preliminary spectral classification type (see Sect. 4.1.1)
Column 8: Alternative names taken from the NED[2].

The spectra of all emission-line galaxies are shown in the Appendix.

The results of line flux measurements are given in Table 2. It contains the following information:
Column 1: The object's IAU-type name with the prefix HS.
Column 2: Observed flux (in 10^{-16} erg s^{-1} cm^{-2}) of the Hβ λ 4861 Å line.
Columns 3, 4, 5: The observed flux ratios [OII]/Hβ, [OIII]/Hβ and Hα/Hβ. For objects without detected Hβ emission line, the absolute fluxes are given.
Columns 6, 7: The observed flux ratios [NII] λ 6583 Å/Hα, and ([SII] λ 6716 Å + [SII] λ 6731 Å)/Hα.
Columns 8, 9, 10: Equivalent widths of the lines [OII] λ 3727 Å, Hβ and [OIII] λ 5007 Å.

4.1.1. Classification criteria

The emission-line galaxies are classified using the line ratio diagnostic diagrams proposed by Baldwin et al. (1981, hereafter BPT81) and Veilleux & Osterbrock (1987, hereafter VO87). These diagrams allow to distinguish between narrow-line AGN ionization by a non-thermal power law continuum and HII-region-like galaxies with ionization of gas by a large number of hot OB-stars.

According to VO87 a confident separation of the two ionization mechanisms and a classification of the galaxy can be obtained from its location on the [OIII] λ 5007 Å/Hβ versus [NII] λ 6583 Å/Hα diagram. This diagram has the advantage of being reddening-insensitive and is used to classify the ELGs from the Calar Alto observations which cover a wide spectral region from 3700 Å to 8100 Å.

The observations of the 12 ELGs with the 6 m telescope do not cover the red region. For these objects we use the [OIII] λ 5007 Å/Hβ versus [OII] λ 3727 Å/[OIII] λ 5007 Å diagram, which is also a good constraint on the ionization mechanisms, but it is reddening-sensitive, so that extinction corrections would be desirable. However this correction is unreliable for the 6 m telescope observations due to poor S/N ratios near the Hγ emission line. Nevertheless for high-excitation BCGs the average reddening is not large (Izotov et al. 1993a, 1994, 1997b), and therefore, even without extinction correction they occupy nearly the correct positions in this diagnostic diagram. For lower-excitation galaxies, however, the reddening is getting larger in average, and thus the possible uncertainty of their classification can increase, especially if an object falls into the transition area.

In Fig. 4 emission-line galaxies from the HSS sample are plotted in comparison with some BCGs from the SBS (Izotov et al. 1994, 1997b; Thuan et al. 1995) and ELGs from the Case survey (Weistrop & Downes 1988, 1991; Augarde et al. 1987; Salzer et al. 1995; Ugryumov et al. 1998). The branch of HII-galaxies is separated from AGN by a short-dashed line running in both figures from the left-top corners populated by objects showing strong emission lines to the right-bottom corners populated by objects with a low level of gas ionization.

It is clear from the data in Fig. 4 that the major part of the observed HSS emission-line galaxies belongs to HII-galaxies and only a few objects can be classified as probable AGN.

From the two objects in the AGN region of Fig. 4a only one — HS 1609+4902 — can be definitely classified in both diagrams as a Sy2 galaxy. The second probable AGN-type object is HS 1304+4710. In Fig. 4a it is located not too far from the border line separating HII-type objects from AGNs. We tentatively classify it as a possible LINER (low-ionization nuclear emission-line region galaxies; Heckman 1980). In Fig. 4b this object falls however within the HII-type region. A possible reason for this is the reddenning due to the dust extinction.

Among the second priority candidates we find a number of low-excitation massive galaxies with nondetected (in low S/N spectra) Hβ and [OIII] λ 5007 Å emission lines. They are tentatively classified as possible LINERs (marked as LINER? in Table 1) according to the flux ratios of [NII] λ 6583 Å and Hα (Heckman 1980). Although these galaxies are not shown in Fig. 4, they, likely, populate the extreme right-bottom corner in Fig. 4a.

We use some additional criteria for the classification of ELGs in the cases where the S/N ratio is insufficient

[2] The NASA/IPAC Extragalactic Database (NED) is operated by the Jet Propulsion Laboratory, California Institute of Technology, under contract with the National Aeronautics and Space Administration.

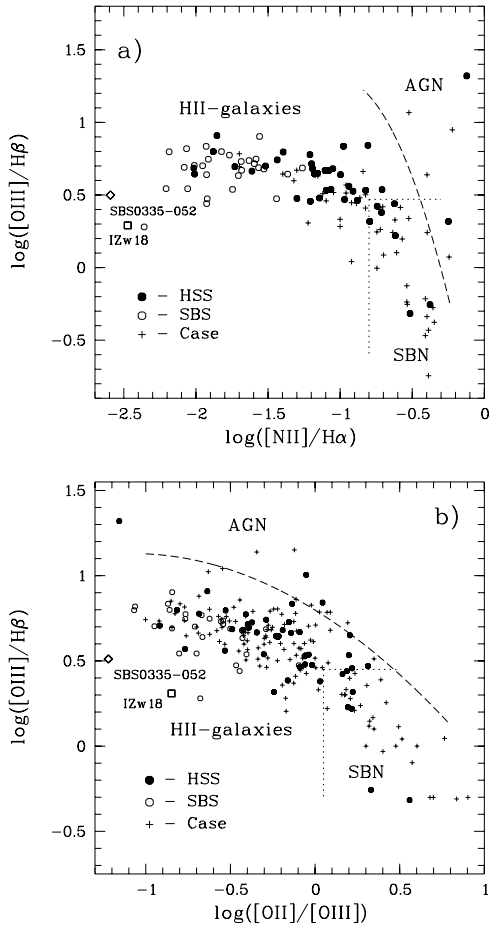

Fig. 4. a, b) Classification diagrams for ELGs. The dashed line separates regions of HII-type and AGN spectra, according to VO87 and BPT81. The dotted lines separate the region in which high $T_{\rm eff}$ star excitation takes place from the region of low ionization populated by DANS and SBN (after S89a)

to use the diagnostic diagrams. As it was emphasized by Salzer (1989a, hereafter S89a) there is a tight correlation between the ELG type and their mean global parameters such as luminosity and size. In particular, the ELGs with the highest excitation are low-luminosity, compact objects, while AGN-type objects are almost always high-luminosity, large galaxies.

Two more objects in Fig. 4b, HS 1038+4616 and HS 1443+5018, fall into AGN region. We suspect that it is due to poor S/N ratio for Hβ. Therefore, their large [OIII] λ 5007 Å/Hβ ratios are unreliable, and, probably these galaxies are low excitation BCGs. Indeed, their low luminosities ($M_B = -17\overset{\rm m}{.}2$ and $-17\overset{\rm m}{.}1$, respectively) are more compatible with a HII-type nature.

HII-galaxies can be splitted further into several classes depending on physical parameters such as sizes, absolute magnitudes, colors, metal abundance, equivalent widths (EW) of the [OIII] λ 5007 Å line and morphology. S89a have proposed the following sequence of HII-galaxy types (starting with the least luminous and most compact objects and ending with the most luminous, quite large spirals): "Sargent–Searle (SS) objects" (or "Blue Compact Dwarfs (BCD)"), "dwarf HII hotspot (DHIIH) galaxies", "HII hotspot (HIIH) galaxies", "Dwarf Amorphous Nucleus Starburst (DANS) galaxies" and "Starburst Nucleus (SBN) galaxies". There is also a significant correlation of the luminosity with other parameters, such as metallicity, EW of the [OIII] λ 5007 Å line and color.

The insufficient quality of our spectroscopy does not allow to perform such detailed classification. Therefore, in our case SS, DHIIH and HIIH galaxies are taken together as one class of blue compact/HII galaxies (BCGs), which are objects with strong and moderate emission lines, caused by the large number of young OB-stars in current burst of star formation.

Following S89a, we separate the BCGs and low-excitation ELGs regions in the diagnostic diagrams with dotted lines (Fig. 4). This border is derived from the analysis and generalization of good-quality ELG observational data from the UM survey[3]. To classify objects near the border we use additional parameters, such as EW([OIII] λ 5007 Å) and M_B, according to their characteristic values for corresponding ELGs from S89a.

4.1.2. Selection effects

The main ELG candidate selection criteria applied here are a blue continuum (near λ 4000 Å) and the presence of strong or moderate [OIII] $\lambda\lambda$ 4959, 5007 Å emission lines recognized in digitized prism spectra with magnitudes in the range $B = 16\overset{\rm m}{.}0 - 19\overset{\rm m}{.}5$. Figure 5 shows the equivalent widths of the [OIII] λ 5007 Å line versus the apparent and absolute blue magnitudes. It is evident from Fig. 5a that the detection limit of the HSS for BCGs based on this strongest emission line is EW([OIII] λ 5007 Å) $\leq$ 15 Å. There is a clear trend of increase of equivalent widths (EW) with apparent magnitude, and even more noticeable anticorrelation between EWs and absolute magnitudes, if not only BCGs but all ELGs are taken into account. Similar trends were noticed for the UM ELGs by Salzer et al. (1989a,b).

In analogy to the UM ELGs, the anticorrelation evident in Fig. 5b is caused by two effects. First, because of

[3] There is one more method to disentangle well hot star and shock wave excitation in ELGs with the help of diagnostic diagrams, where the [OI] λ 6300 Å line is incorporated. As mentioned already by Heckman (1980) as well as by BPT81 and VO87 this is probably the best method to distinguish between the three mechanisms of activity in ELGs. The disadvantage of this method is that for low-quality spectra this weak emission line cannot be measured.

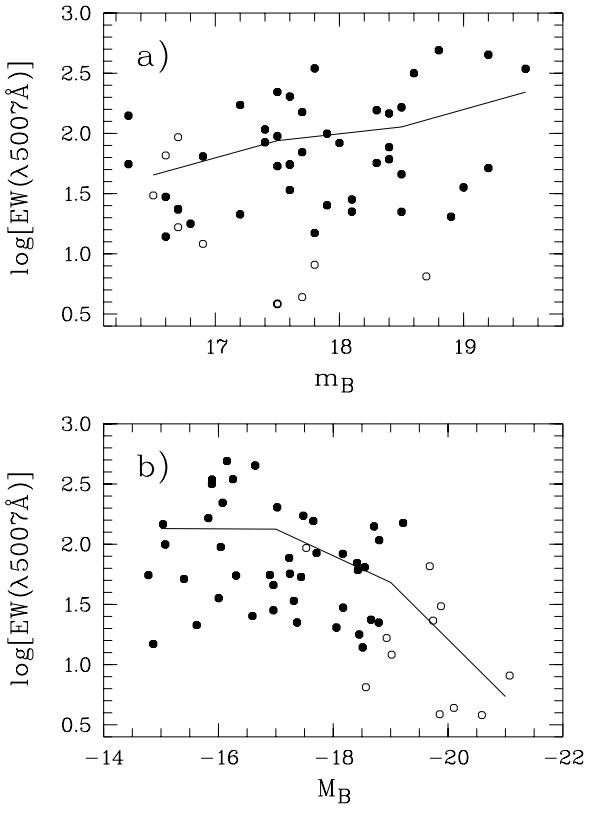

Fig. 5. **a, b)** Logarithm of the equivalent width of [OIII] λ 5007 Å emission line versus blue apparent **a)** and absolute magnitudes **b)** for HSS ELGs. BCG are plotted as filled circles and other types as empty circles. The solid line joins averages of equivalent widths taken over 1 mag apparent magnitude intervals **a)** and over 2 mag absolute magnitude intervals **b)**

the brightness limit imposed by the plates we miss low-luminosity ELGs with weak emission lines. The galaxies would populate the lower left corner of the Fig. 5b. Second, the region of avoidance in the upper right corner is most likely caused by metallicity effects. In general HII-regions in bright galaxies have larger heavy element abundance, and, therefore, they are cooler with lower EW([OIII] λ 5007 Å).

4.2. Quasars

QSOs with strong emission lines might be selected in our sample if either the Lyα λ 1216 Å line redshifted to $z \sim 3$ or the MgII λ 2798 Å line redshifted to $z \sim 0.9$ appear in the wavelength region between 5000 Å and the sensitivity break of the Kodak IIIa-J photoemulsion near 5400 Å. This produces an easily visible emission peak on the digitized prism spectra even for very faint objects ($B \sim 19\overset{m}{.}0 - 20\overset{m}{.}0$) which is usually hard to distinguish from low-redshifted [OIII] features.

Both kinds of QSOs are present in our sample (Table 3): HS 1313+4651 with $z \sim 3$, and HS 1446+4611 and HS 1300+4835 with $z \sim 0.8$. The fourth QSO (HS 1040+4904) might have been a distant ELG because the feature visible in the objective prism spectrum was thought to be [OII] λ 3727 Å emission line shifted to a wavelength near 4000 Å. However, the slit spectrum suggests that an identification with MgII λ 2798 Å emission line at $z \sim 0.5$ is more likely.

4.3. Objects without emission lines

4.3.1. Absorption-line galaxies

The signal-to-noise ratio of spectra for seven bright non-ELG galaxies is sufficient to detect absorption lines, allowing the determination of redshifts. These galaxies are listed in Table 4.

Taking into account a probable underestimation of their apparent brightnesses by 1 magnitude, they are (with one exception) quite luminous, with M_B in the range $-19\overset{m}{.}0$ to $-20\overset{m}{.}5$. Most of them have noticeable Hβ and Hγ absorption and so they are probably post-starburst galaxies.

4.3.2. Stellar objects

To separate stellar spectra from other non emission-line spectra we use a template with the most common stellar features which is cross-correlated with the observed spectra. We found 111 objects with definite stellar spectra. Six of them are obvious M-stars. The remaining stellar spectra are roughly classified as A – G stars, most of them having intermediate types between A and F, or F and G. The coordinates, apparent magnitudes, spectral types and lists of absorption features identified in the spectra of these objects are given in Table 5.

4.3.3. Non-classified objects

The spectra of 24 objects show neither emission nor absorption features and, therefore, cannot be classified. We divide them into three categories according to the slope of their continuum in the range between 4000 and 5000 Å. Six objects (25%) have "blue" spectra ($\alpha(4000-5500) \leq -0.2$), 10 objects (42%) have "flat" spectra ($-0.2 \leq \alpha(4000-5000) \leq +0.2$) and 8 objects (33%) are "red" objects ($\alpha(4000-5000) \geq +0.2$). Thus, if these non-classified objects are stars, most of them are rather hot.

One of the non-classified objects observed with the 6 m telescope (HS 1517+4021) has a quite strange spectrum in the range $3700 - 5500$ Å, indicating a possible composite system. On the DSS (Digital Sky Survey) we find an indication of a close faint companion star, which could have entered into IPCS circular aperture.

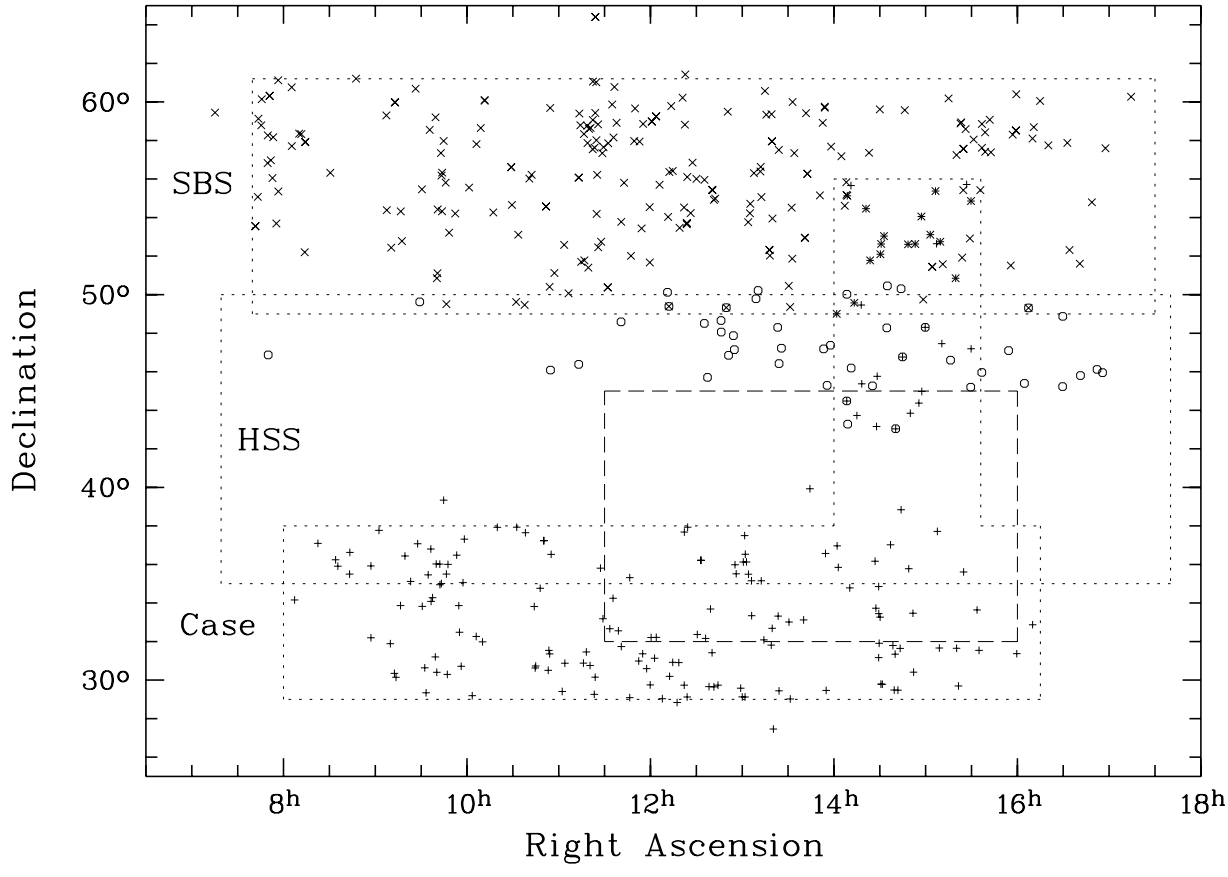

Fig. 6. Sky projection of the BCGs from the HSS sample (o) together with BCGs from the zones of SBS (x) and Case surveys (+). The dashed box delineates one of the regions of the Heidelberg void survey (Popescu et al. 1996, 1997)

5. Discussion

5.1. Survey efficiency and fraction of BCGs

The principles, methods, selection procedures and first follow-up spectroscopy results of the Hamburg/SAO survey described in the previous sections are intended to create a new large and deep sample of BCGs. Summarizing the data and their preliminary analysis presented in Sects. 3 and 4 we conclude that the selection technique used in this paper is efficient in search for objects with strong and moderate [OIII] $\lambda\lambda$ 4959, 5007 Å emission lines. However, the overall detection efficiency of emission-line objects is rather low for this first sample (about 31%). In Sect. 5.3 we discuss additional selection criteria which can improve the ELGs detection efficiency.

The fraction of BCGs (as our main goal) among all emission-line objects is ∼63% (47 BCGs among 74 in total). This is significantly larger than the fraction of all HII-type objects among ELGs in the UCM (33%) (Gallego et al. 1997) and larger than ∼50% in the UM sample (DHIIH, HIIH and SS-objects in S89a).

The preliminary estimate of the mean surface number density of BCGs found in the HSS is about 0.21 BCG/square degree, accounting all HII-type objects selected as first and second priority candidates in the band centered at $\delta = +47.5°$ with the range of $\alpha = 12^h - 17^h$. The estimate incorporates 38 BCGs in the indicated region from this paper and 21 objects obtained independently from the HSS, which either are known as HII-galaxies from earlier publications (Vogel et al. 1993; Popescu et al. 1996; Schneider et al. 1994), or have been observed later by us and will be presented in forthcoming papers, or are among several of our unpublished BCGs in and near the SBS zone. This estimate is still a lower limit since not all first priority HSS candidates in this region are observed. This value is similar to that for the BCG sample in the zone of the SBS survey (0.24 BCG/square degree; Thuan et al. 1994) and for the sample of BCGs from the region 3 of Popescu et al. (1996).

Due to our selection criteria cut-off of luminous galaxies, we reduce significantly the fraction of Sy galaxies in comparison with the above mentioned surveys (< 2% here versus 10% in the UM sample and 8% in the UCM sample) and pick up only the low-luminosity tail of AGN (possible LINERs) mainly as interlopers and second priority candidates. The detection of a significant fraction of possible

LINERs (6 galaxies or 8%) is surprising, and has no clear explanation. The remaining discovered ELGs are probable SBN and DANS (22%).

It is interesting to note that due to the limit in redshift, the faintest ELG candidates are mainly also the least luminous, and thus they are expected to be typical BCGs. This is reflected by the statistics of all detected ELGs. For the ranges of $m_B = 16^{\rm m} - 17^{\rm m}$, $17^{\rm m} - 19^{\rm m}$ and $19^{\rm m} - 20^{\rm m}$ the fraction of BCGs is about 57%, 67% and 80%, respectively. This was also noticed by Ugryumov et al. (1998) in the study of Case ELG candidates. It gives us an additional impetus to search for emission–line candidates down to the very limits of the plates.

5.2. Aspects of spectral classification, chemistry and metallicity

We already discussed in Sect. 4.1.1, that the ELGs are classified according to their positions in the line ratio diagnostic diagrams.

A comparison of the positions of the new HSS ELGs in these diagrams shows that our classification appears to be self-consistent for all BCGs, and, therefore, is rather reliable.

It is interesting to compare the positions in diagnostic diagram of the new HSS BCGs with those of the well studied BCGs from the SBS sample (Izotov et al. 1994, 1997b; Thuan et al. 1995). Most of the SBS BCGs populate the region with $\log([\mathrm{N\,II}]\,\lambda 6583\,\mathrm{\AA}/\mathrm{H}\alpha) < -1.2$ (Fig. 4). About 20% of the HSS BCGs are located in the same region. The real fraction of such BCGs with high excitation HII-regions will be quantified after better quality spectroscopic observations. At least 2 HSS BCGs with high excitation HII-regions are present in the SBS list ($\delta = 49^\circ - 50^\circ$) and they are independently rediscovered in the present study. In particular, our line flux ratios for HS 1249+4919 ($\log(\mathrm{O/H})+12 = 7.72$) are very close to those from Thuan et al. (1995).

The region with $\log([\mathrm{N\,II}]\,\lambda 6583\,\mathrm{\AA}/\mathrm{H}\alpha) < -2$ contains the BCGs with the lowest metallicities. We discover two new HSS BCGs located in this region. Hence low metallicity objects can be selected by our search method.

5.3. Improvement of selection criteria

Having quite low efficiency at this pilot stage it is natural to try to improve the selection criteria. The analysis of all accumulated data discussed here, shows that in order to improve the selection of BCGs the following additional criteria and selection procedures should be applied to the preselected lists of candidates:

1. Second priority candidates have very low detection rates for BCGs ($< 20\%$) and pick up mainly ELGs of other types which are not in the focus of our project. So, these objects should not be observed further except as backup sample. This will result in an underestimate of the BCG surface density of $\lesssim 20\%$.
2. It appears that the majority of bright ($m_B < 18\overset{\rm m}{.}0$) stellar-like objects are either blue or M-dwarf stars. Thus, additional examination of candidates on direct images in order to discriminate between stellar and fuzzy images will allow to remove most of the obvious brighter star-type interlopers.
3. The results of follow-up spectroscopy have shown that even part of the prominent first priority candidates turned out non-emission objects. Subsequent check of the plate material have shown that some defects or strong noise peaks looked like strong emission features on objective prism spectra. Thus, we concluded that it is necessary to make a careful check of all first priority candidates on the original spectral plates (scanning of 2 plates of the same region with cross-check — in the majority of cases) or additional visual inspection of the candidate spectra — in case of only one plate — to remove possible dust grains and noise hits.

These improvements allow to increase the discovery rate of BCGs by a factor of ∼2, as it is shown in a forthcoming paper by Pustilnik et al. (1998).

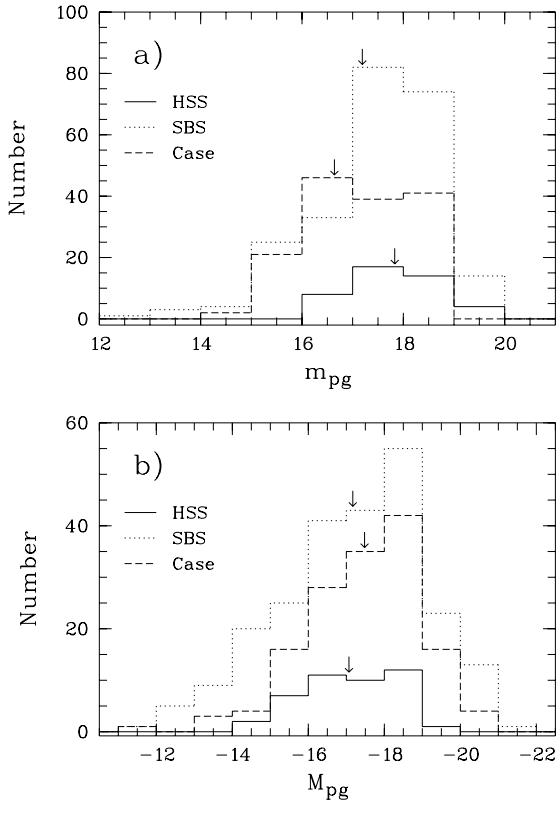

Fig. 7. Histograms of apparent **a)** and absolute **b)** photographic magnitudes for three BCGs samples: new HSS BCGs from this paper, BCGs from the SBS sample (Pustilnik et al. 1995) and Case BCGs from Ugryumov et al. (1998), Ugryumov (1997). The arrows indicate the mean magnitude for each sample

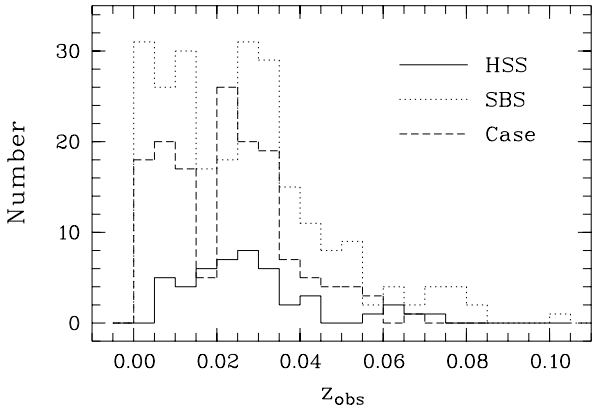

Fig. 8. Histograms of redshift distributions for the same BCG samples, as for the previous figure

5.4. The statistical properties of HSS BCGs

The sky distribution of the BCGs from the HSS sample is shown in Fig. 6 together with BCGs from the SBS and Case surveys (Izotov et al. 1993b; Pustilnik et al. 1995; Ugryumov 1997; Ugryumov et al. 1998). Our aim is to create a large sample (the Northern BCG sample) in this whole area of about 3000 square degrees. For this it is important to understand how the properties of the objects in these three samples compare to each other. First, we compare the apparent magnitude distributions of the three samples. For the HSS BCG sample we use the data of the 47 BCGs found in this first part of the survey. We consider it as representative (excluding the brighter part of the sample, which will be discussed later). An abrupt decrease of the number of objects in the magnitude range between $m_B = 18\overset{\mathrm{m}}{.}0$ and $19\overset{\mathrm{m}}{.}0$ is present in the distributions of all three samples (Fig. 7) although the fraction of galaxies in this magnitude range is different in each sample. As it was shown by Pustilnik et al. (1995) the BCG sample in the SBS zone can be considered as rather complete up to $m_{\mathrm{pg}} = 18\overset{\mathrm{m}}{.}0$. The similar behaviour of the faint end of the apparent magnitude distributions infers that the Northern BCG sample may have a similar completeness down to this limiting magnitude. It is evident from Fig. 7 that there is a significant deficit in the HSS of galaxies with $m_B \leq 16\overset{\mathrm{m}}{.}0$ caused by the adopted limits in the parameter space of the selection criteria. Additionally, several known bright emission-line galaxies are found in the HSS, but not observed in this work. These selection constraints lead to a difference between the mean apparent magnitudes of HSS BCGs and the BCGs of the two other samples. The real brightness distribution of HSS BCGs will be discussed in more detail in later papers.

Despite of the differences in the apparent magnitude distributions, the absolute photographic magnitude distributions for the same BCG samples shown in the histograms of Fig. 7 look much more similar and have similar mean luminosities. This may indicate that the contents of all three BCG samples are the same.

The radial velocity distributions shown for the same BCG samples in Fig. 8 have similar break values of the redshift (about 0.035), at which a significant fall-off takes place. This again reflects the similar limiting apparent magnitudes of all three samples. The absence of nearby HSS objects in this histogram is artificial, because the bright BCGs with known velocities were not observed here. For the sake of clarity it should be noted that galaxies were selected in SBS both through UV-excess and emission lines. The BCG sample however was exclusively selected from emission-line candidates. Therefore the redshift distribution of the SBS is similar to the other two samples. The similarities of BCG properties in the HSS, SBS and Case surveys imply that the galaxies from these surveys can be combined into a larger sample to study the spatial distribution of BCGs in this area. A first comparison of the luminosity function which can be derived from these different samples can be found in Hopp (1998).

6. Conclusions

We conducted follow-up spectroscopy for a pilot sample of the Hamburg/SAO Survey for emission-line galaxies. The spectroscopy resulted in the detection or/and quantitative spectral classification of 74 emission-line objects. Of them 55 are newly discovered, and 19 are already known in the literature. For 8 of the latter the redshifts are determined at first time, and for most of the rest emission line ratios are presented at first time. Summarizing the presented description of the selection procedure, the follow-up spectroscopy results and their discussion we conclude:

- The methods used for the selection of ELG candidates on objective prism plates give a sufficiently high fraction of BCGs in the resulting lists of detected ELGs (47 galaxies or 63%), in accordance with the original aim of the Hamburg/SAO survey project.
- Besides of BCGs we found also 4 new quasars and 23 ELGs of other types.
- The overall detection efficiency of emission-line objects for the pilot sample is rather low (about 31%) and should be improved. The performed analysis of the data allowed to formulate additional selection criteria.
- The estimated lower limit of the mean surface number density of BCGs is about 0.21/square degree, similar to that for the BCG samples from the SBS and from the ELG sample in the direction of voids.
- A preliminary comparison of the brightnesses and redshifts of the newly discovered BCGs with those from the samples in the SBS and Case survey zones shows that they are quite similar and thus their combination will create a new homogeneously selected large BCG sample, suitable for the study of the spatial distribution of BCGs.

Acknowledgements. This work was supported by the grant of the Deutsche Forschungsgemeinschaft No. 436 RUS 17/77/94. A.V.U. is very grateful to the staff of the Hamburg Observatory for their hospitality and kind assistance. SAO authors appreciate the partial financial support from the RFBR grant No. 96-02-16398 and from Russian Center of Cosmoparticle Physics "Cosmion". The partial support of this work by the INTAS grant No. 96-0500 is acknowledged. We acknowledge the partial support of this project by Russian Ministry of Science and Technology for 6 m telescope of SAO RAS (BTA, reg. number 01-43). U.H. acknowledges the support by the SFB 375 Astroteilchenphysik of the Deutsche Forschungsgemeinschaft. The authors thank the anonymous referee for useful notes helping to improve the text. This research has made use of the NASA/IPAC Extragalactic Database (NED).

References

Augarde R., Figon P., Kunth D., Sevre P., 1987, A&A 185, 4
Baldwin J.A., Phillips M.M., Terlevich R., 1981, PASP 93, 5
Bardeen J.M., Bond J.R., Kaiser N., Szalay A.S., 1986, ApJ 304, 15
Boroson T.A., Salzer J.J., Trotter A., 1993, ApJ 412, 524
Davies J.I., Phillips S., 1989, Ap&SS 157, 291
Drabek S.V., Kopylov I.M., Somov N.N., Somova T.A., 1986, Izvestia SAO 22, 64
Dekel A., Silk J., 1986, ApJ 303, 39
Engels D., Cordis L., Köhler T., 1994, Proc. IAU Symp. 161, MacGillivray H.T. (eds.). Kluwer, Dordrecht, p. 317
Gallego J., Zamorano J., Rego M., Vitores A.G., 1997, ApJ 475, 502
Hagen H.-J., Groote D., Engels, D., Reimers D., 1995, A&AS 111, 195
Haro G., 1956, Bol. Obs. Tonantzintla y Tacubaya 14, 329
Heckman, 1980, A&A 87, 152
Hopp U., 1998, Proc. "Ringberg Workshop on Large Scale Structure", Hamilton E. (ed.) (in press)
Izotov Yu.I., Lipovetsky V.A., Guseva N.G., Kniazev A.Yu., Stepanian J.A., 1990, Nat 343, 238
Izotov Yu.I., Guseva N.G., Lipovetsky V.A., et al., 1993a, Astron. Astrophys. Trans. 3, 179
Izotov Yu.I., Lipovetsky V.A., Guseva N.G., 1993b, in: "The Feedback of Chemical Evolution on the Stellar Content of Galaxies", Alloin D. & Stasinska G. (eds.), p. 127
Izotov Yu.I., Thuan T.X., Lipovetsky V.A., 1994, ApJ 435, 647
Izotov Y.I., Lipovetsky V.A., Chaffee F.H., et al., 1997a, ApJ 476, 698
Izotov Yu.I., Thuan T.X., Lipovetsky V.A., 1997b, ApJS 108, 1
Kniazev A.Yu., 1994, SAO internal report No. 223
Kunth D., Matteucci F., Marconi G., 1995, A&A 297, 634
Maddox S.J., Efstathiou G., Sutherland W.J., 1990, MNRAS 246, 433
Markarian B.E., 1967, Afz 3, 55
Markarian B.E., Lipovetsky V.A., Stepanian J.A., 1983, Afz 19, 29
Markarian B.E., Stepanian J.A., Erastova L.K. 1987, Proc. IAU Symp. 121, Byurakan, Armenia, USSR, Khachikian E.Y., Fricke K.J., Melnik J. (eds.), p. 25
Markarian B.E., Lipovetsky V.A., Stepanian J.A., Erastova L.K., Shapovalova A.I., 1989, Comm. Special Astrophys. Obs. 62, 5
Massey P., Strobel K., Barnes J.V., Anderson E., 1988, ApJ 328, 315
Maza J., Ruiz M.T., González L.E., Wischnjewsky M., Peña M., 1991, A&AS 89, 389
Mazzarella J.M., Balzano V.A., 1986, ApJS 62, 751
Pesch P., Stephenson C.B., MacConnell D.J., 1995, ApJS 98, 41
Popescu C.C., Hopp U., Hagen H.-J., Elsässer H., 1996, A&AS 116, 43
Popescu C.C., Hopp U., Elsässer H., 1997, A&A 328, 756
Popescu C.C., Hopp U., Hagen H.J., Elsässer H., 1998, A&AS (in press)
Pustilnik S.A., Ugryumov A.V., Lipovetsky V.A., Thuan T.X., Guseva N.G., 1995, ApJ 443, 499
Pustilnik S.A., Engels D., Ugryumov A.V., Lipovetsky V.A., Hagen H.-J., Kniazev A.Yu., Izotov Yu.I., Richter G., 1998, A&AS (in preparation)
Rosenberg J.L., Salzer J.J., Moody J.W., 1994, AJ 108, No. 5, 1557
Salzer J.J., McAlpine G.M., 1988, AJ 96, 1192
Salzer J.J., MacAlpine G.M., Boroson T.A., 1989a, ApJS 70, 479
Salzer J.J., 1989b, ApJ 347, 152
Salzer J.J., Moody J.W., Rosenberg J.L., Gregory S.A., Newberry M.V., 1995, AJ 109, 2376
Sargent W.L.W., Searle L., 1970, ApJ 162, L155
Searle L., Sargent W.L.W., 1972, ApJ 173, 25
Smith M.G., Aguirre C., Zemelman M., 1976, ApJS 32, 217
Schneider D.P., Schmidt M., Gunn J.E., 1994, AJ 107, No. 4, 1245
Stepanian J.A., 1994, Proc. IAU Symp. 161. Kluwer, Dordrecht, MacGillivray H.T. (ed.), p. 731
Terlevich R., Melnick J., Masegosa J., Moles M., Copetti M.V.F., 1991, ApJ 247, 823
Thuan T.X., Martin G.E., 1981, ApJ 247, 823
Thuan T.X., Alimi J.-M., Gott J.R., Schneider S.E., 1991, ApJ 370, 25
Thuan T.X., Izotov Yu.I., Lipovetsky V.A., Pustilnik S.A., 1994, Proc. ESO/OHP Workshop "Dwarf Galaxies", Meylan & Prugniel (eds.), p. 421
Thuan T.X., Izotov Yu.I., Lipovetsky V.A., 1995, ApJ 445, 108
Ugryumov A.V., 1997, Ph.D. Thesis, SAO RAS
Ugryumov A.V., Pustilnik S.A., Lipovetsky V.A., Izotov Yu.I., Richter G.M., 1998, A&AS 131, 295
Veilleux S., Osterbrock D.E., 1987, ApJS 63, 295
Vogel S., Hagen H.-J., Groote D., et al., 1993, A&AS 98, 193
Weistrop D., Downes R.A., 1988, ApJ 331, 172
Weistrop D., Downes R.A., 1991, AJ 102, No. 5, 1680
Weinberg D.H., Szomoru A., Guhathakurta P., van Gorkom J.H., 1991, ApJ 372, L13
Zamorano J., Rego M., Gallego J., et al., 1994, ApJS 95, 387
Zamorano J., Gallego J.G., Rego M., Vitores A.G., Alonso O., 1996, ApJS 105, 343
Zwicky S., 1964, ApJ 143, 192

Appendix A: Spectra of emission-line galaxies

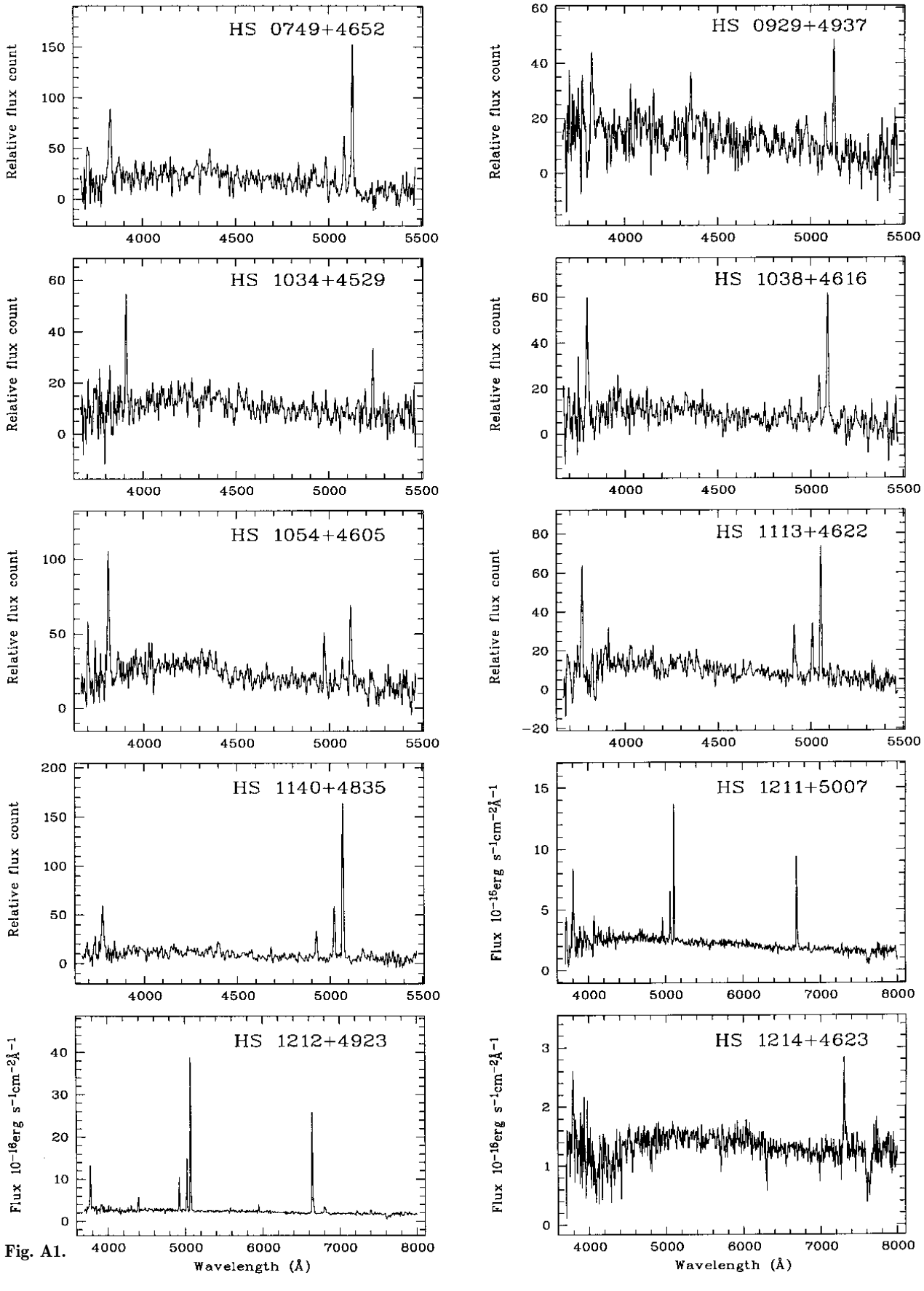

Fig. A1.

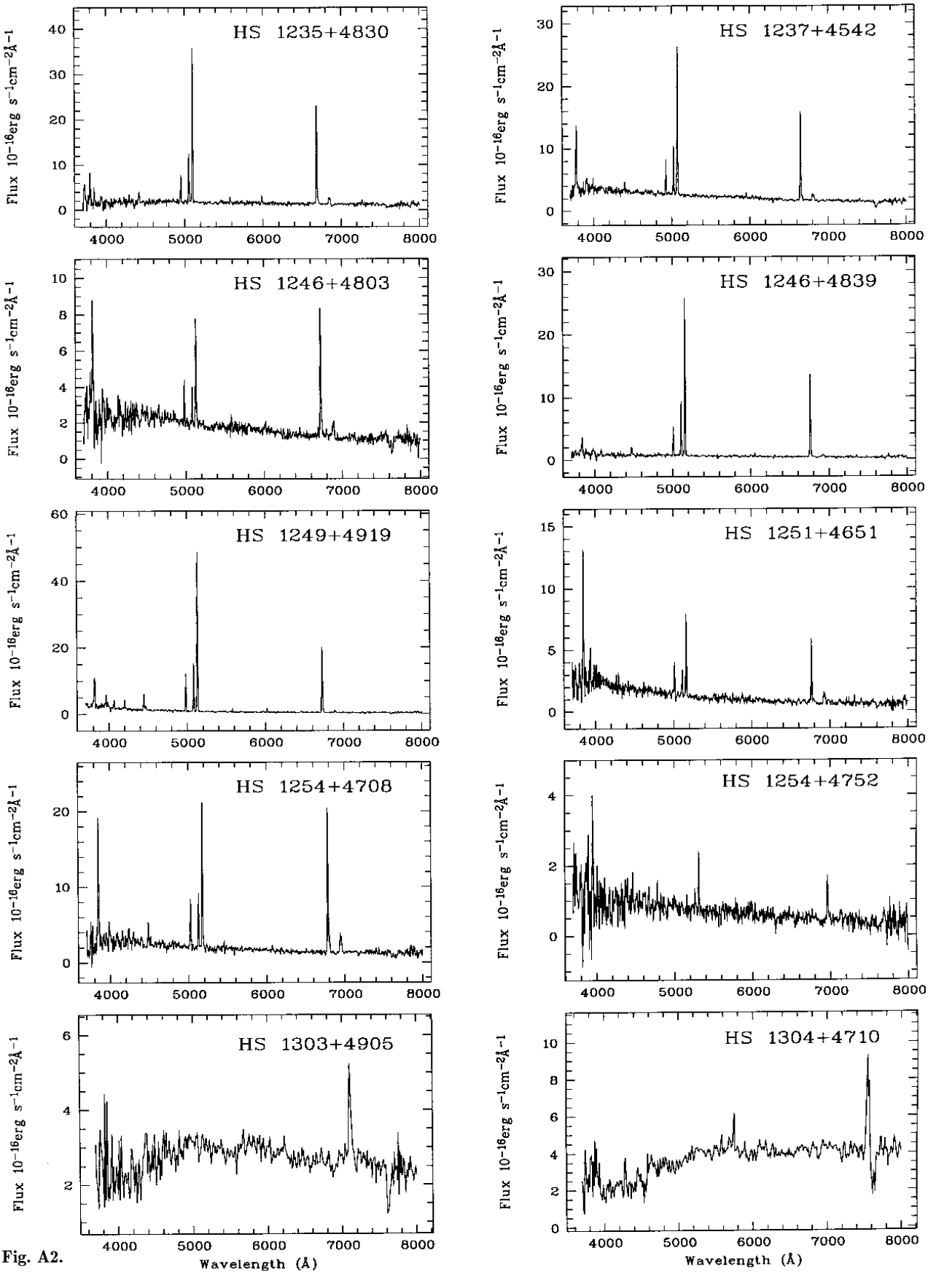
HS 1235+4830
HS 1237+4542
HS 1246+4803
HS 1246+4839
HS 1249+4919
HS 1251+4651
HS 1254+4708
HS 1254+4752
HS 1303+4905
HS 1304+4710
Flux 10⁻¹⁶erg s⁻¹cm⁻²Å⁻¹
Wavelength (Å)

Fig. A2.

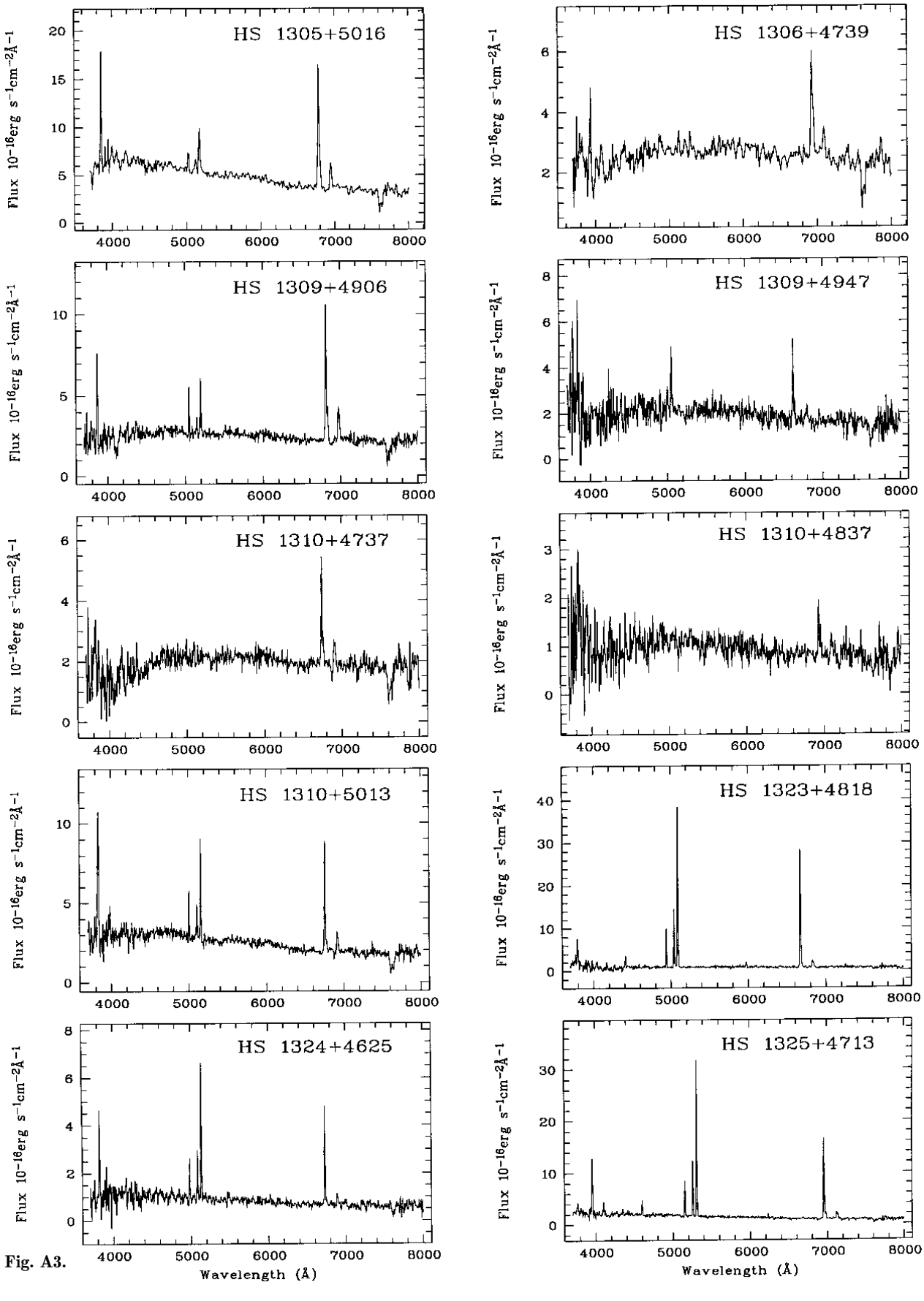
HS 1305+5016
HS 1306+4739
HS 1309+4906
HS 1309+4947
HS 1310+4737
HS 1310+4837
HS 1310+5013
HS 1323+4818
HS 1324+4625
HS 1325+4713
Flux 10⁻¹⁶erg s⁻¹cm⁻²Å⁻¹
Wavelength (Å)

Fig. A3.

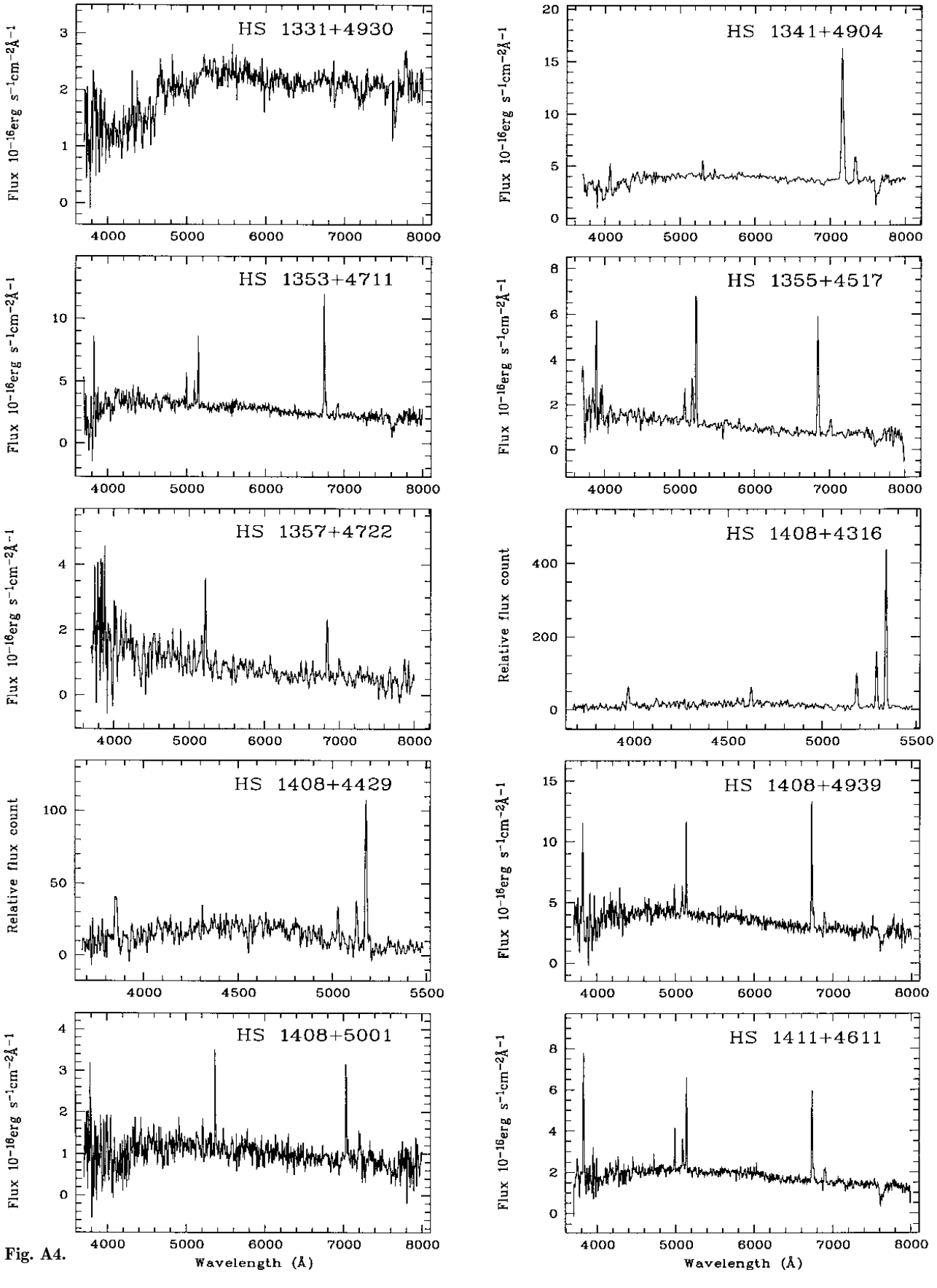
HS 1331+4930
HS 1341+4904
HS 1353+4711
HS 1355+4517
HS 1357+4722
HS 1408+4316
HS 1408+4429
HS 1408+4939
HS 1408+5001
HS 1411+4611
Flux 10⁻¹⁶erg s⁻¹cm⁻²Å⁻¹
Relative flux count
Wavelength (Å)

Fig. A4.

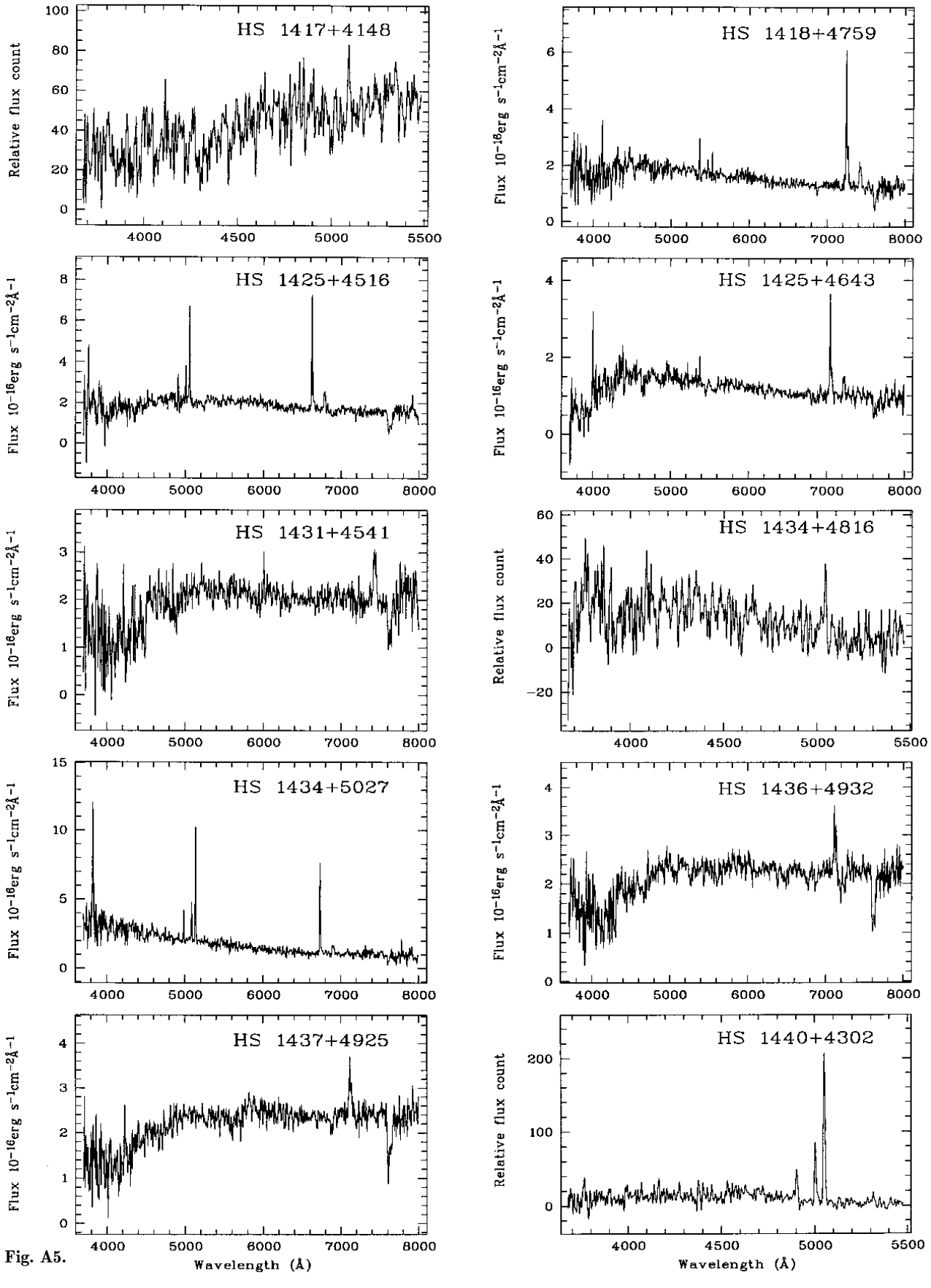
HS 1417+4148
HS 1418+4759
HS 1425+4516
HS 1425+4643
HS 1431+4541
HS 1434+4816
HS 1434+5027
HS 1436+4932
HS 1437+4925
HS 1440+4302
Relative flux count
Flux 10⁻¹⁶erg s⁻¹cm⁻²Å⁻¹
Wavelength (Å)

Fig. A5.

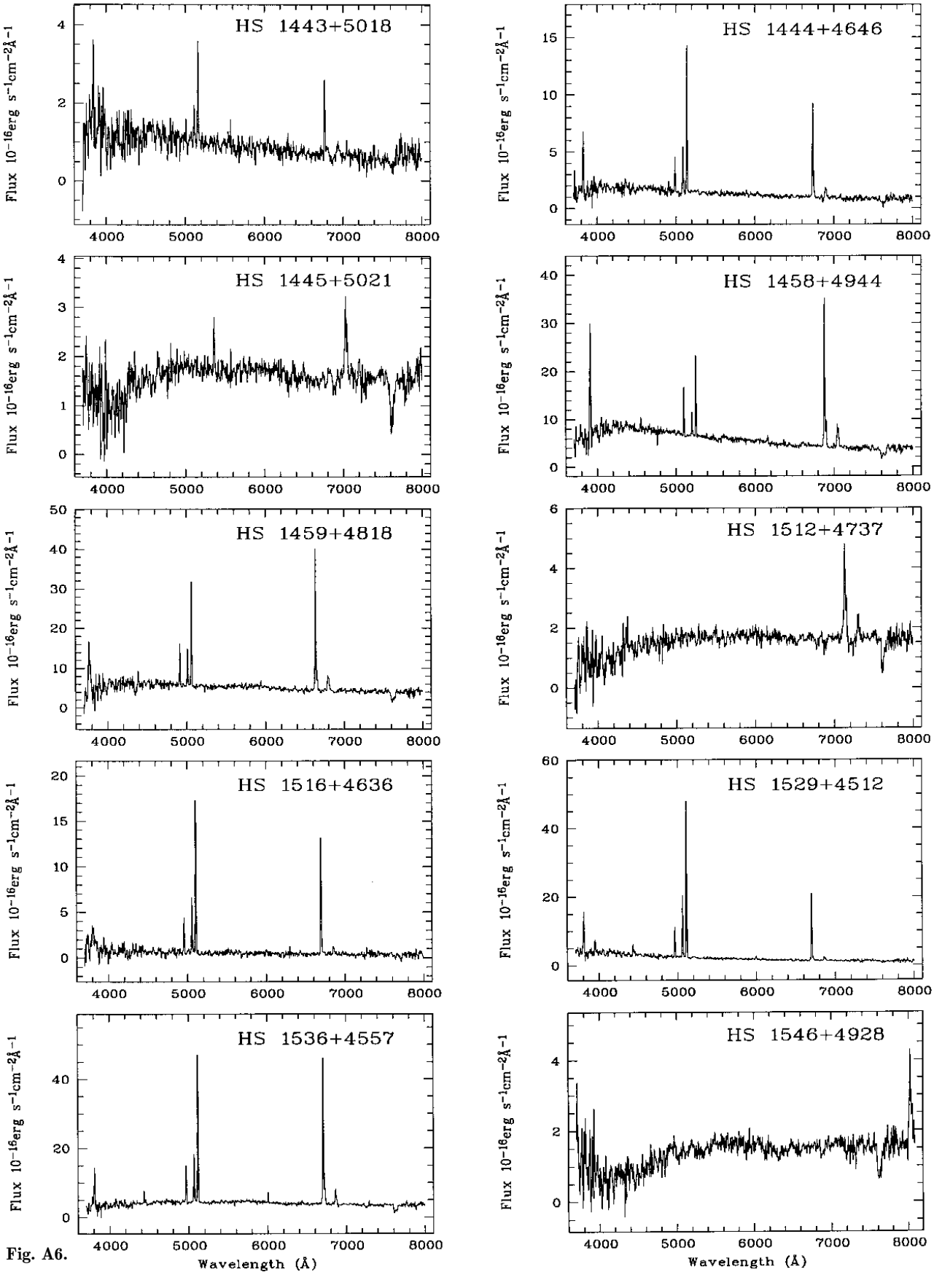
HS 1443+5018
HS 1444+4646
HS 1445+5021
HS 1458+4944
HS 1459+4818
HS 1512+4737
HS 1516+4636
HS 1529+4512
HS 1536+4557
HS 1546+4928
Flux 10⁻¹⁶erg s⁻¹cm⁻²Å⁻¹
Wavelength (Å)

Fig. A6.

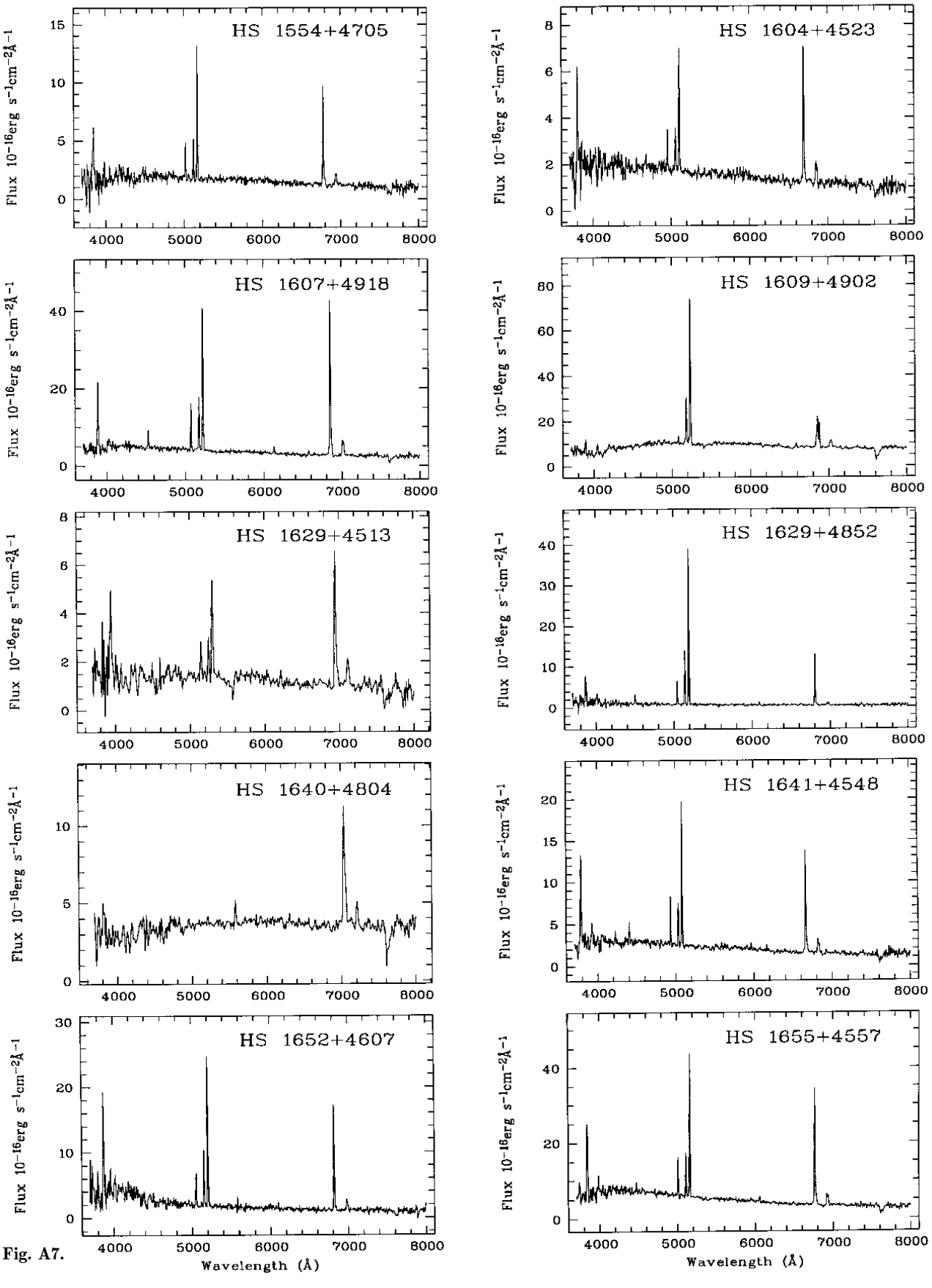
HS 1554+4705
HS 1604+4523
HS 1607+4918
HS 1609+4902
HS 1629+4513
HS 1629+4852
HS 1640+4804
HS 1641+4548
HS 1652+4607
HS 1655+4557
Flux 10^{-16}erg s^{-1}cm^{-2}Å^{-1}
Wavelength (Å)

Fig. A7.